HOKKAIDO UNIVERSITY

Title	Periodontal tissue engineering using an apatite/collagen scaffold obtained by a plasma‐ and precursor‐assisted biomimetic process
Author(s)	Kanemoto, Yukimi; Miyaji, Hirofumi; Nishida, Erika; Miyata, Saori; Mayumi, Kayoko; Yoshino, Yuto; Kato, Akihito; Sugaya, Tsutomu; Akasaka, Tsukasa; Nathanael, Arputharaj Joseph; Santhakumar, Syama; Oyane, Ayako
Citation	Journal of Periodontal Research, 57(1), 205-218 https://doi.org/10.1111/jre.12954
Issue Date	2021-11-16
Doc URL	http://hdl.handle.net/2115/87261
Rights	This is the peer reviewed version of the following article: Kanemoto, Y., Miyaji, H., Nishida, E., Miyata, S., Mayumi, K., Yoshino, Y., Kato, A., Sugaya, T., Akasaka, T., Nathanael, A. J., Santhakumar, S., & Oyane, A. (2022). Periodontal tissue engineering using an apatite/collagen scaffold obtained by a plasma- and precursor-assisted biomimetic process. Journal of periodontal research, 57(1), 205–218., which has been published in final form at 10.1111/jre.12954. This article may be used for non-commercial purposes in accordance with Wiley Terms and Conditions for Use of Self-Archived Versions. This article may not be enhanced, enriched or otherwise transformed into a derivative work, without express permission from Wiley or by statutory rights under applicable legislation. Copyright notices must not be removed, obscured or modified. The article must be linked to Wiley ’ s version of record on Wiley Online Library and any embedding, framing or otherwise making available the article or pages thereof by third parties from platforms, services and websites other than Wiley Online Library must be prohibited.
Type	article (author version)
File Information	2022 Kanemoto J Periodont Res.pdf

Instructions for use

Hokkaido University Collection of Scholarly and Academic Papers : HUSCAP

Periodontal tissue engineering using an apatite/collagen scaffold obtained by a plasma- and precursor-assisted biomimetic process

Yukimi KANEMOTO[1], Hirofumi MIYAJI[1*], Erika NISHIDA[1], Saori MIYATA[1], Kayoko MAYUMI[1], Yuto YOSHINO[1], Akihito KATO[1], Tsutomu SUGAYA[1], Tsukasa AKASAKA[2], Arputharaj Joseph Nathanael[3,A], Syama SANTHAKUMAR[3], Ayako OYANE[3**]

Institutions

[1] Department of Periodontology and Endodontology, Faculty of Dental Medicine, Hokkaido University, N13, W7, Kita-ku, Sapporo, Hokkaido 060-8586, Japan

[2] Department of Biomedical Materials and Engineering, Faculty of Dental Medicine, Hokkaido University, N13 W7, Kita-ku, Sapporo, Hokkaido 060-8586, Japan

[3] Nanomaterials Research Institute, National Institute of Advanced Industrial Science and Technology (AIST), Central 5, 1-1-1 Higashi, Tsukuba, Ibaraki 305-8565, Japan

[A] Currently working at Centre for Biomaterials, Cellular and Molecular Theranostics (CBCMT), India

***Corresponding authors**

Hirofumi MIYAJI, DDS, PhD.

Department of Periodontology and Endodontology, Faculty of Dental Medicine, Hokkaido University, N13, W7, Kita-ku, Sapporo, Hokkaido 060-8586, Japan.

E-mail: miyaji@den.hokudai.ac.jp

****Co-corresponding authors**

Ayako OYANE, PhD.

Nanomaterials Research Institute, National Institute of Advanced Industrial Science and Technology (AIST), Central 5, 1-1-1 Higashi, Tsukuba, Ibaraki 305-8565, Japan

E-mail: a-oyane@aist.go.jp

Key words

Bone augmentation, cyto-compatibility, dog class II furcation defect model,

immunohistochemistry, low-crystalline apatite, osteogenic differentiation, periodontal healing.

Abstract

Background and objectives

In the treatment of severe periodontal destruction, there is a strong demand for advanced scaffolds that can regenerate periodontal tissues with adequate quality and quantity. Recently, we developed a plasma- and precursor-assisted biomimetic process by which a porous collagen scaffold (CS) could be coated with low-crystalline apatite. The apatite-coated collagen scaffold (Ap-CS) promotes cellular ingrowth within the scaffold compared to CS in rat subcutaneous tissue. In the present study, the osteogenic activity of Ap-CS was characterized by cell culture and rat skull augmentation tests. In addition, the periodontal tissue reconstruction with Ap-CS in a beagle dog was compared to that with CS.

Methods

The plasma- and precursor-assisted biomimetic process was applied to CS to obtain Ap-CS with a low-crystalline apatite coating. The effects of apatite coating on the scaffold characteristics (i.e., surface morphology, water absorption, Ca release, protein adsorption, and enzymatic degradation resistance) were assessed. Cyto-compatibility and the osteogenic properties of Ap-CS and CS were assessed in vitro using preosteoblastic MC3T3-E1 cells. In addition, we performed in vivo studies to evaluate bone augmentation and periodontal tissue reconstruction with Ap-CS and CS in a rat skull and canine furcation lesion, respectively.

Results

As previously reported, the plasma- and precursor-assisted biomimetic process generated a low-crystalline apatite layer with a nanoporous structure that uniformly covered the Ap-CS surface. Ap-CS showed significantly higher water absorption, Ca release, lysozyme adsorption, and collagenase resistance than CS. Cell culture experiments revealed that Ap-CS was superior to CS in promoting the osteoblastic differentiation of MC3T3-E1 cells while suppressing their proliferation. Additionally, Ap-CS significantly promoted (compared to CS) the augmentation of the rat skull bone and showed the potential to regenerate alveolar bone in a dog furcation defect.

Conclusion

Ap-CS fabricated by the plasma- and precursor-assisted biomimetic process provided superior promotion of osteogenic differentiation and bone neoformation compared to CS.

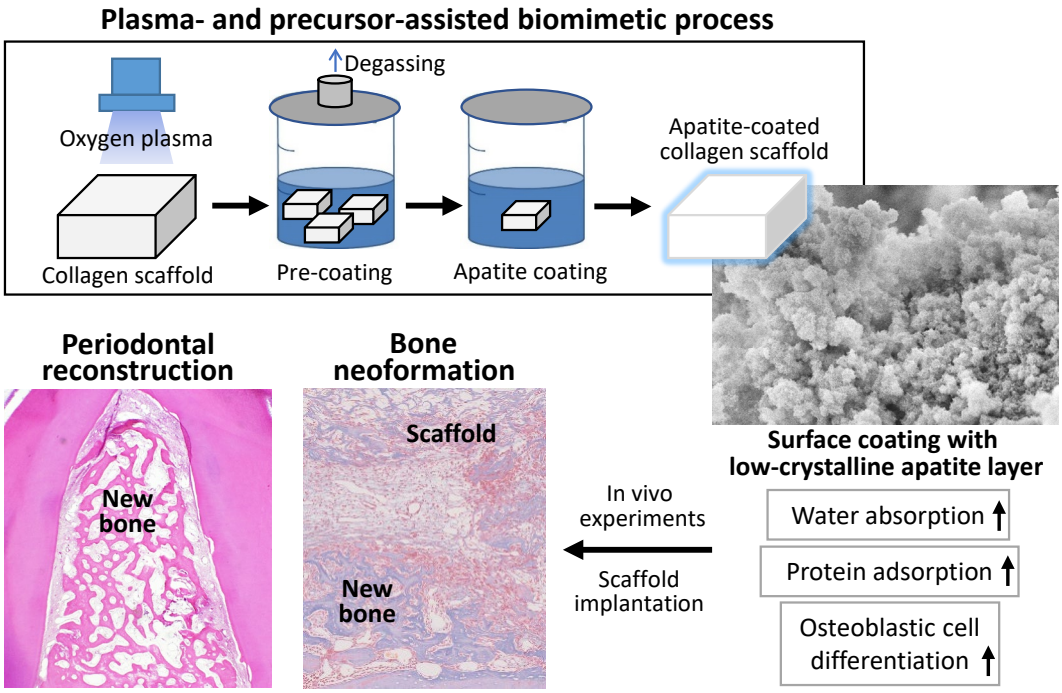

Graphic abstract

1. Introduction

Periodontal disease by infection with periodontal pathogens frequently induces inflammatory responses that result in the severe destruction of the periodontal tissue, including alveolar bone, related to tooth supporting system. The goal of periodontal tissue engineering is to regenerate lost soft and hard tissues using three elements[1)]: cells[2-4)], growth factors[5-8)], and scaffolds[9-11)]. Among these three elements, scaffolds take a key role in tissue engineering by inducing tissue responses, such as cell proliferation and differentiation, vascular network construction, and extracellular matrix secretion, thereby regenerating a three-dimensional functional tissue[12)]. Although various scaffolds have been developed, none has achieved sufficient periodontal regeneration in the case of severe periodontal tissue destruction. Therefore, a scaffold with advanced functionality is required for periodontal regenerative therapy.

Sintered calcium phosphates (CaPs), such as hydroxyapatite (HA) and β-tricalcium phosphate (β-TCP), have been used clinically as osteoconductive scaffolds, given their compositional similarity to human bone minerals[13, 14)]. These bioceramics have the advantages of biocompatibility and osteoconductivity[15, 16)], but have the disadvantage of slow bioresorbability. Sintered HA is rarely resorbed after implantation and remains in the body for a long time[17-19)]. Despite being categorized as bioresorbable ceramics, β-TCP can remain in the body for over half of a year[20, 21)]. Bone defects created by periodontal disease are located close to oral cavity; to reduce infection risk, a scaffold should be rapidly resorbed while being replaced with the regenerated bone tissue.

Natural bone shows a hierarchical structure consisting of low-crystalline apatite crystals deposited on a three-dimensional network of collagen matrices[22)]. Therefore, it is expected that a similar nanocomposite, i.e., a low-crystalline apatite-coated collagen

network, would be beneficial as a scaffold for bone regeneration[23]. It is known that low-crystalline apatite can be coated on a substrate using an acellular supersaturated CaP solution as a coating medium, a process that resembles in vivo bone apatite formation. The resulting low-crystalline apatite exhibits good osteogenic cell compatibility, as well as higher biodegradability compared to sintered HA ceramics[24]. The low-crystalline apatite coating process using supersaturated CaP solutions (biomimetic process) is a mild liquid-phase method; hence, this process can be carried out at normal temperature and pressure, and can be used with low-melting-point substrates including organic polymers. These are notable advantages to the biomimetic process compared to commonly used CaP coating processes such as plasma spraying[25, 26], pulse laser deposition[27, 28], and sputtering methods[29, 30]. Oyane et al. previously developed a relatively simple biomimetic technique, the plasma- and precursor-assisted biomimetic process[31]. In this process, a substrate is treated with oxygen plasma for surface activation, dipped alternately in Ca and P solutions for precoating with amorphous CaP (a precursor of apatite), and then immersed in a supersaturated CaP solution for low-crystalline apatite coating. Those authors succeeded in low-crystalline apatite coating of various materials, including porous blocks[32], fibers[33], and sponges[34] , by use of the plasma- and precursor-assisted biomimetic process.

Recently, Nathanael et al. created a three-dimensional collagen scaffold (CS) coated with low-crystalline apatite using the plasma- and precursor-assisted biomimetic process[35]. The apatite-coated collagen scaffold (Ap-CS) promoted cell-ingrowth into the scaffold compared to the uncoated CS in rat subcutaneous tissue[35]. We hypothesized that Ap-CS should promote osteogenic differentiation, bone formation, and periodontal regeneration compared to CS. The aim of the present study was to perform in-depth characterization of Ap-CS to verify our hypothesis and to demonstrate the potential utility

of Ap-CS for periodontal tissue engineering. In vitro cell culture tests were carried out to elucidate the osteogenic properties of Ap-CS. Bone augmentation by Ap-CS was examined after implantation onto the rat skull. In addition, periodontal reconstruction by Ap-CS was investigated in an experimental canine furcation defect model. The results obtained with Ap-CS were compared to those obtained with CS.

2. Materials and Methods

2.1. Preparation of CS and Ap-CS

Ap-CS (Figure 1A, right) was prepared from CS (Figure 1A, left) by the plasma- and precursor-assisted biomimetic process (Figure 2) as described previously[35]. CS was prepared by cutting a sheet of calf atelocollagen (Terudermis®, Olympus Terumo Biomaterials Corp., Tokyo, Japan) into rectangular pieces (6 mm × 6 mm × 3 mm, Figure 1A, left). CS was treated with oxygen plasma to increase the hydrophilicity of the surface. The plasma treatment was carried out under an O_2 gas (Takachiho Chemical Industrial Co., Ltd., Tokyo, Japan) pressure of 30 Pa for 30 seconds with a power density of 0.1 W/cm^2, using an ion etching system (FA-1, Samco Inc., Kyoto, Japan). Three pieces of the plasma-treated CS were immersed in 30 mL of a 200 mM $CaCl_2$ solution, washed with 30 mL of ultrapure water, and then immersed in 30 mL of a 200 mM $K_2HPO_4 \cdot 3H_2O$ solution for precoating with amorphous CaP. A vacuum degassing system was employed to fill and exchange the solutions throughout the interconnected porous structure of the scaffold, as detailed in the previous report[35].

The scaffolds (3 pieces) were removed from the 200 mM $K_2HPO_4 \cdot 3H_2O$ solution, rinsed with a supersaturated CaP solution (CP solution), and each piece was subsequently immersed in 30 mL of the CP solution for 48 hours at 25 °C to permit the amorphous CaP

to grow into low-crystalline apatite. The CP solution was prepared by dissolving reagent-grade NaCl (final concentration = 142 mM), $K_2HPO_4 \cdot 3H_2O$ (1.50 mM), HCl (40 mM), and $CaCl_2$ (3.75 mM) sequentially in ultrapure water. The pH of the solution was adjusted to a final value of 7.4 at 25 °C using tris(hydroxymethyl)aminomethane (50 mM) and the required amount of 1 M HCl. All of the reagents used for preparation of the CP solution were purchased from Nacalai Tesque, Inc., Kyoto, Japan. After immersion in the CP solution for 48 hours, the scaffold was washed with ultrapure water and freeze-dried in a lyophilizer (Model DC41, Yamato Scientific Co., Ltd., Japan, and FDS-1000, Tokyo Rikakikai Co., Ltd., Tokyo, Japan) to finally obtain Ap-CS (Figure 1A, right).

2.2 Physicochemical characterization

2.2.1. Scanning electron microscope (SEM) observation

Each piece of CS and Ap-CS was halved to expose its inner surface of the scaffold. The nano-micro scale structures of the outer and cut (inner) surfaces of CS and Ap-CS were observed by SEM (S-4800; Hitachi, Ltd., Tokyo, Japan) at accelerating voltage of 10 kV after Pt-Pd coating.

2.2.2. Water absorption test

Water absorption capacity of CS and Ap-CS was assessed as described previously[36]. Each piece of CS and Ap-CS was weighed and immersed in sterile distilled water (Otsuka Pharmaceutical Co., Ltd., Tokyo, Japan) for 30 minutes at room temperature. After wiping excess water from the scaffold using Whatman filter paper (GE Healthcare Japan Co., Ltd., Japan), the scaffold was weighed again to quantify the amount of absorbed water.

2.2.3. Calcium-releasing test

Calcium (Ca) release from CS and Ap-CS was assessed. Each piece of CS and Ap-CS was immersed in 0.5 mL of phosphate-buffered saline (PBS, FUJIFILM Wako Pure Chemical Corp., Osaka, Japan) at 37 °C for 7 days. The amount of released Ca in PBS was measured using a calcium test kit (calciumE-test; FUJIFILM Wako Pure Chemical Corp.) and spectrophotometer (U-1100; Hitachi, Ltd.) at 610 nm.

2.2.4. Protein adsorption test

Protein adsorption on CS and Ap-CS was assessed using anionic bovine serum albumin (FUJIFILM Wako Pure Chemical Corp.) and cationic lysozyme hydrochloride from egg white (FUJIFILM Wako Pure Chemical Corp.). Portions (50 μg) of each protein were dissolved (separately) in 100 μL of distilled water; the resulting solutions were absorbed by each piece of CS and Ap-CS under reduced pressure. Subsequently, the scaffold was immersed into 1.0 mL of deionized distilled water to permit leaching of unbound and weakly bound protein. After stirring for 10 minutes, the protein content leached from the scaffold into the water was measured using a total protein kit (Micro Lowry, Peterson's Modification; Sigma-Aldrich Co., St Louis, MO, USA) in combination with a spectrophotometer at 610 nm. The amount of each protein adsorbed onto CS and Ap-CS was calculated by subtracting the protein content leached in the water from the applied total dose.

2.2.5. Enzymatic degradation test

To assess the collagenase resistance of CS and Ap-CS, each piece was weighed and

then immersed in 1 mL of PBS supplemented with 1% collagenase type I (0.1 mg/mL; FUJIFILM Wako Pure Chemical Corp.) for 3 hours at 37 °C. After the collagenase treatment, the residual scaffold was dehydrated using absolute ethanol, air-dried, and weighed. The enzymatic degradation rate was calculated from the weight loss of the scaffold following collagenase treatment.

2.3. Cell culture experiments

2.3.1. Cyto-compatibility assessments

Mouse-derived osteoblastic MC3T3-E1 cells (5×10^4; RIKEN BioResource Center, Tsukuba, Japan) were inoculated onto CS and Ap-CS in 48-well plates and cultured in a humidified 5% CO_2 atmosphere at 37 °C. The culture medium was a mixture of the following reagents purchased from Thermo Fisher Scientific Inc. (Waltham, MA, USA): minimum essential medium (alpha-GlutaMAX™-I), 10% qualified fetal bovine serum, and 1% penicillin/streptomycin. After incubation for 1, 3, 5, or 7 days, a water-soluble tetrazolium salt-8 (WST-8) assay and a lactate dehydrogenase (LDH) assay were carried out using Cell Counting Kit-8 (Dojindo Laboratories, Mashiki, Japan) and Cytotoxicity LDH Assay Kit-WST (Dojindo Laboratories), respectively. In both assays, the absorbance was measured using a microplate reader (ETY-300, Toyo Sokki Co., Ltd., Japan).

To assess cell adhesion, MC3T3-E1 cells (7×10^3) were seeded onto CS and Ap-CS, cultured in 48-well plates for 24 hours, and fixed with 3.5% formaldehyde. The cells were treated at 4 °C overnight with F-actin probe (1.5 μg, Actistain 555 Fluorescent Phalloidin; Cytoskeleton, Inc., Denver, CO, USA) and nuclear staining dye (2 μg, 4’,6-diamidino-2-phenylindole, Dojindo Laboratories) according to the manufacturer’s instructions. The

cells then were observed with a fluorescence microscope (Biorevo BZ-9000, Keyence Corp., Osaka, Japan).

In addition, MC3T3-E1 cells (2×10^3) were inoculated onto CS and Ap-CS in 48-well plates and cultured for 24 hours. The live and dead cells were stained respectively with LIVE/DEAD Viability/Cytotoxicity Kit for mammalian cells (Thermo Fisher Scientific Inc.) and observed by fluorescence microscopy.

2.3.2. Real-time reverse transcription-polymerase chain reaction (RT-PCR) assays

MC3T3-E1 cells (1×10^6) were seeded on CS and Ap-CS placed in 48-well plates and cultured for 14 days under the same conditions as in Section 2.3.1. The medium was replaced every 2 days. After culturing for 14 days, total RNA was extracted from the cultured cells using TRIzol (Invitrogen, Carlsbad, CA, USA). RNA (1 μg) was used for reverse transcription. The resulting cDNA was amplified with ReverTra Ace-α FSK-101 (Toyobo Co., Ltd., Osaka, Japan). Primers (Applied Biosystems, Carlsbad, CA, USA) were used to target the following osseous marker genes: *alkaline phosphatase* (*Alp*, Mm00475834_m1), *integrin-binding sialoprotein* (*Ibsp*, Mm00492555_m1), and *bone gamma carboxyglutamate protein 1* (*Bglap1*, Mm03413826_m1). As a control, the housekeeping gene *glyceraldehyde-3-phosphate dehydrogenase* (*Gapdh*, Mm99999915_g1) also was targeted. Real-time RT-PCR was carried out using an ABI Prism 7300 sequence detection system (Applied Biosystems) and the resulting data were standardized to *Gapdh* expression using the 2-ΔΔCt method[37-38].

2.4. In vivo experiments

2.4.1. Animals

Animal experiments using rats and beagle dog were performed in accordance with the institutional animal use and care regulations of Hokkaido University. All procedures were approved by the Animal Research Committee of Hokkaido University (Approval Numbers: 16-29 for the rat experiment and 19-84 for the dog experiment). Fourteen Wistar rats (male, 10 weeks old, weighing 190–210 g each) and 1 Beagle dog (female, 12 months old, weighing approximately 10 kg) were used in this study. For general anesthesia, we used a mixture of three drugs: midazolam (Dormicum; Astellas Pharma, Inc., Tokyo, Japan), medetomidine hydrochloride (Domitor; Nippon Zenyaku Kogyo Co., Ltd., Koriyama, Japan), and butorphanol tartrate (Vetorphale; Meiji Seika Pharma Co., Ltd., Tokyo, Japan). The doses of midazolam, medetomidine hydrochloride, and butorphanol tartrate in the mixture were 2.0, 0.15, and 2.5 μg/kg for rat (respectively) and 0.15, 0.04, and 0.15 μg/kg for dog (respectively). Local anesthesia was performed using 2% lidocaine hydrochloride with 1:80,000 epinephrine (Xylocaine Cartridge for Dental Use; Dentsply Sirona K.K., Tokyo, Japan).

2.4.2. Implantation in a rat skull

CS and Ap-CS were implanted in a rat skull using the onlay grafting technique[16] for the bone augmentation test. After general anesthesia was applied, the rat skull was exposed, and cortical bone with a size of 4 mm × 4 mm was removed by dental bur (Maillefer steel round bur; Dentsply Sirona K.K., Tokyo, Japan) under irrigation with saline (Otsuka Pharmaceutical Factory, Inc., Tokushima, Japan) (Figure 1B, left). A piece of CS or Ap-CS was impregnated with physiological saline and placed onto the skull to fully cover the decorticated region (Figure 1B, right). The skin was repositioned and securely sutured, and tetracycline hydrochloride ointment (Achromycin Ointment; POLA

Pharma Inc., Tokyo, Japan) was applied to the wound. The rats implanted with CS and Ap-CS were referred to as CS and Ap-CS groups, respectively.

2.4.3. Histological observation

Four rats (2 for each group) at 10 days after implantation were euthanized by perfusion with 4% formaldehyde via the aorta after general anesthesia. The extracted rat skulls were decalcified in 10% ethylenediaminetetraacetic acid (EDTA), embedded in paraffin, and sliced. The resulting tissue sections were stained with hematoxylin–eosin (HE), Masson's trichrome (MT), and tartrate-resistant acid phosphatase (TRAP). In addition, immunohistochemical staining was conducted. After thermal epitope retrieval (by heating at 95 °C in citrate buffer (pH 6) or Tris-EDTA buffer (pH 9)), the sections were incubated overnight with the following primary antibodies: mouse anti-CD68 (1:100 dilution; Bio-Rad Laboratories, Inc., Hercules, CA), mouse anti-CD163 (1:150 dilution; Bio-Rad Laboratories, Inc.), mouse anti-runt-related transcription factor 2 (RUNX2) (1:200 dilution; Abcam plc., Cambridge, UK), and rabbit anti-osteocalcin (OCN) (1:200 dilution; Proteintech Group, Inc., Chicago, IL). Antigen–antibody reaction sites were detected by Red Cy3 (Jackson Immuno-Research, Inc., West Grove, PA). Nuclear staining was performed using SYTOX Green nucleic acid stain (Thermo Fisher Scientific Inc.). The stained tissue sections were observed using fluorescence microscopy.

2.4.4. Histometric measurement

After 35 days of implantation, 10 rats (5 per group) were euthanized to prepare HE-stained tissue sections (as described in Section 2.4.3). The sections were observed with a light microscope for histomorphometric measurements of the area and height of the newly

formed bone, and of the area of the residual scaffold, using image analysis software (Image J 1.41; National Institutes of Health, Bethesda, MD, USA).

2.4.5. Implantation in an experimental periodontal defect in dog

To evaluate periodontal reconstruction with Ap-CS, a pilot experiment was conducted using a dog periodontal furcation defect model. Following general anesthesia, buccal mucogingival flaps were elevated to expose the mandibular alveolar bone, and class II buccal furcation defects (5 mm in height and 3 mm in horizontal width) were created in the second, third, and fourth premolars (Figure 1C, left)[9, 11]. The defects including the furcation and buccal cortical bone defect regions had a depth of approximately 5-6 mm. After planing of the exposed root facing the furcation defects, the defects were filled with a piece of CS or Ap-CS, and the sites were referred to as CS or Ap-CS groups, respectively. Upon implantation, a piece of CS or Ap-CS was impregnated with physiological saline and compressed to fulfill the defect (Figure 1C, right). Ap-CS was applied to the furcation of the second and fourth premolars in the right teeth row, and the third premolar in the left teeth row. CS was applied to the rest of the furcations. The flaps then were repositioned and sutured.

2.4.6. Micro-computed tomography (micro-CT) and histological assessments

After 35 days of implantation, the dog was euthanized via perfusion fixation by 10% buffered formalin under general anesthesia. Tissue blocks including premolar furcations were removed and observed using a micro-CT scanner (Latheta LCT-200, Hitachi, Ltd.). The area of the radiopaque region (regarded as the calcified bone region) in each furcation was measured using ImageJ, and the bone volume was calculated as a

percentage of the furcation volume.

Subsequently, the tissue blocks were decalcified in 10% formic acid, embedded in paraffin, and sliced along the mesio-distal plane to prepare HE-stained periodontal tissue sections. The resulting sections were observed using light microscopy. The areas of the newly formed bone and furcation defect were measured using ImageJ, and the bone area was calculated as a percentage of the furcation area.

2.5. Statistical Analysis

For each quantitative parameter, mean and standard deviation were calculated. Statistical differences were analyzed using two-tailed non-paired Student‘s t-tests (for comparisons between two group) and two-tailed One-way ANOVA with post hoc Turkey HSD test (for comparisons among three or more groups) using SPSS 11.0 (IBM Corporation, Armonk, NY, USA); results with $P < 0.05$ were considered statistically significant.

3. Results

3.1. Physicochemical characterization

SEM images of the outer and inner surfaces of CS and Ap-CS are shown in Figure 3. As shown in the lower-magnification image, CS consisted of filament- and sheet-like collagen struts and possessed a microporous structure. The higher magnification image of CS showed a smooth surface of the sheet-like collagen. In contrast, Ap-CS showed nanostructured depositions on its outer and inner surfaces. These nanostructured depositions should be low-crystalline apatite, according to the results of previous energy dispersive X-ray spectroscopy and X-ray diffraction analysis[35)].

The amounts of water absorbed by CS and Ap-CS were 60.0 ± 4.0 and 98.3 ± 5.9 mg, respectively. Thus, the amount of water absorbed by Ap-CS was 1.6-fold that absorbed by CS ($P<0.01$, Figure 4A). The amount of Ca released from Ap-CS was 0.66 ± 0.15 mg, whereas that from CS was under the detection limit ($P<0.01$, Figure 4B). In the protein adsorption test, the amounts of adsorbed anionic albumin and cationic lysozyme were 14.7 ± 3.3 and 32.4 ± 4.5 μg for CS (respectively) and 17.9 ± 4.5 and 42.5 ± 6.2 μg for Ap-CS (respectively). Thus, the amount of lysozyme adsorbed to Ap-CS was significantly larger than that adsorbed to CS ($P<0.05$, Figure 4C). In the enzymatic degradation test, the weights before and after the collagenase treatment were 4.39 ± 0.43 and 0.76 ± 0.13 mg for CS (respectively) and 7.72 ± 1.49 and 6.04 ± 1.21 mg for Ap-CS (respectively). Thus, the degradation rate of CS (82.8 ± 1.8%) was significantly greater than that of Ap-CS (21.9 ± 2.7%) ($P<0.01$, Figure 4D).

3.2. Cyto-compatibility assessments

Fluorescence images of the osteoblastic MC3T3-E1 cells cultured on CS and Ap-CS after F-actin and LIVE/DEAD BacLight staining are shown in Figure 5A. F-actin staining revealed that the cells adhered to the struts of both CS and Ap-CS (red staining). LIVE/DEAD staining showed that most of the cells on CS and Ap-CS stained green, indicating that these cells were alive.

The results of cyto-compatibility assessments are presented in Figure 5B. In the WST-8 assay, there was no significant difference in WST-8 activities of the cells between the CS and Ap-CS groups after culturing for 1 day. WST-8 activities of the cells cultured on CS increased with increasing culture period up to 7 days. In contrast, WST-8 activities of the cells cultured on Ap-CS remained constant for 7 days, and were significantly lower

than those of the cells cultured for 3-7 days on CS ($P<0.05$). In the LDH assay, the cells cultured on CS and Ap-CS showed equivalent LDH activities on Days 1 and 7. On Days 3 and 5, the cells cultured on Ap-CS showed higher LDH activities compared to those of cells cultured on CS ($P<0.05$).

3.3. Real-time RT-PCR assessments

Real-time RT-PCR demonstrated that the cells cultured on Ap-CS showed approximately two-fold higher expression of the osseous markers *Alp*, *Ibsp*, and *Bglap1* than did cells cultured on CS, although the difference in the *Alp* expression was not statistically significant (Figure 5C).

3.4. In vivo assessments at 10 days after implantation in a rat skull

Histological images of the rat skull at 10 days after implantation of CS and Ap-CS are shown in Figure 6. The images of HE-stained and MT-stained sections showed that new bone (indicated by NB) was formed continuously on the pre-existing bone (indicated by PB) after implantation of CS and Ap-CS, and residues of these scaffolds were found close to the newly formed bone. In addition to these apparent residues of CS and Ap-CS, fibrous structures similar to the filament-like collagen struts found in pristine CS (Figure 3) were observed inside the trabeculae of new bone, suggesting that these scaffolds were incorporated (in part) into the newly formed bone. In both CS and Ap-CS groups, osteoblast-like and osteoclast-like cells were abundantly observed in the peripheral region of the new bone. This result was further supported by the data for the TRAP-stained sections, which revealed that TRAP-positive osteoclasts also were abundant in the same areas in both the CS and Ap-CS groups. However, TRAP-positive cells were observed

only rarely in the inner region of the residual scaffolds in both groups.

In addition to the optical microscopic observation, fluorescence microscopic observation was carried out following CD68, CD163, RUNX2, and OCN immunostaining (in which the targets were stained red). Macrophages expressing CD68 were observed within and around the residue of Ap-CS more frequently than around the CS residue. CD163-positive macrophages were rarely observed in CS sections, but were observed in large numbers in the inner region of the Ap-CS residue. In the CS group, cells expressing the osteogenic markers RUNX2 and OCN were abundantly observed around the new bone, but were observed rarely inside the CS residue. In the Ap-CS group, RUNX2- and OCN-positive cells were observed not only in the peripheral region of the new bone but also in the inner region of the Ap-CS residue.

3.5. In vivo assessments at 35 days after implantation in a rat skull

Histological images of the rat skull at 35 days after implantation of CS and Ap-CS are shown in Figure 7A. In the HE-stained tissue section of the CS group (upper row of Figure 7A), large residues of CS remained on the cranial bone. Newly formed bone was slight in amount and insufficient to repair fully the bone defect. The high-magnification image revealed that the residue of CS contained few cells. In contrast, a remarkable amount of new bone was observed in sections of the Ap-CS group (lower row of Figure 7A). New bone tissue was augmented from the pre-existing skull bone. High-magnification images showed that the new bone contained osteoblastic cells and a bone marrow structure. Little Ap-CS residue was detected, and the fibrous connective tissue (indicated by FT) overlaying the new bone was rich in cells and blood vessel-like structures.

Histometric measurements revealed that the new bone area and height in the Ap-CS group were significantly greater (4.6-fold in bone area and 2.8-fold in bone height) than those in the CS group ($P<0.05$, Figure 7B). The area of the residual Ap-CS was significantly smaller than that of the residual CS ($P<0.01$).

3.6 In vivo assessments at 35 days after implantation in a dog periodontal defect

The micro-CT and histological images of the dog periodontal tissue at 35 days after implantation of CS and Ap-CS are shown in Figure 8A and B. In the micro-CT images (Figure 8A), the Ap-CS group showed larger radiopaque area (calcified area) at the furcation of the premolar than did the CS group. This observation was supported by histological evaluation (Figure 8B): the HE-stained tissue images showed that the furcation defect was only partially filled with the regenerated alveolar bone in the CS group, whereas most of the defect was filled with the regenerated bone in the Ap-CS group. Both groups showed repair of the periodontal attachment, including the cementum and periodontal ligament. Ankylosis between the alveolar bone and tooth root was not apparent in either of the groups.

The results of quantitative evaluation of the micro-CT and HE-stained tissue images are shown in Figure 8C. The percentages of the bone volume among the furcation volume of the CS and Ap-CS groups (obtained from the micro-CT images) were 66.9 ± 8.4 and 87.6 ± 3.2%, respectively; this difference was statistically significant ($P<0.05$). The percentages of the bone area among the furcation area of the CS and Ap-CS groups (obtained from the HE-stained tissue images) were 54.4 ± 10.6 and 81.7 ± 4.0%, respectively. There was a significant difference between Ap-CS and CS groups ($P<0.05$).

4. Discussion

Ap-CS with low-crystalline apatite coating was prepared using the plasma- and precursor-assisted biomimetic process[35]. As shown by SEM (Figure 3), the nanostructured apatite coating covered both the outer and inner surfaces of the porous collagen scaffold, resulting in the formation of a bone-like organic-inorganic composite (Ap-CS), as reported previously[35]. Apatite coating throughout the porous collagen scaffold was achieved by the liquid-phase coating process (precursor-assisted biomimetic process) in combination with a vacuum degassing system (Figure 2). In this process, the apatite content of a scaffold can be increased further by changing the coating conditions, e.g. by prolonging the coating time or increasing the degree of supersaturation of the CP solution. However, the thickening of the apatite coating narrows residual interconnected pores of the scaffold, which may inhibit cell infiltration and nutrient supply within the scaffold. Thus, the coating conditions were determined so as to produce apatite coating on the entire surface of the porous collagen scaffold while retaining its microporous structure[35].

The apatite coating on Ap-CS was partially degradable in PBS, as verified by the Ca-release test (Figure 4B). This degradation reflects the fact that non-sintered apatite synthesized in liquid medium has poor crystallinity and higher solubility than those of sintered HA. In the enzymatic degradation test, Ap-CS exhibited higher resistance to collagenase degradation than did CS without coating (Figure 4C). This difference was expected, given that the apatite coating on Ap-CS functions as a protective cover, retarding degradation of the underlying collagen by blocking the enzymatic reaction with collagenase.

Surface affinity of a scaffold with water and proteins influences biological

responses to the scaffold[39-41]. Thus, water absorption and protein adhesion tests were carried out as part of the present study. In the water absorption test, Ap-CS absorbed more water than did CS (Figure 4A), suggesting that the apatite coating on Ap-CS increased surface hydrophilicity of the scaffold. The narrowed pore size of the scaffold (owing to the apatite coating) also may influence the increased water absorption of Ap-CS by enhancing water penetration into the porous scaffold via capillary action. In the protein adhesion test, adsorption of the anionic protein albumin was comparable for both CS and Ap-CS (Figure 4C). On the other hand, the adsorbed amount of the cationic protein lysozyme was greater with Ap-CS than with CS. We postulate that the apatite coating on Ap-CS provides more protein-adsorption sites on the scaffold due to the protein-binding capability of apatite[42] and the large surface area of the nanostructured coating. These physicochemical properties of Ap-CS are likely to be beneficial for the use of Ap-CS as a tissue engineering scaffold, as verified by the in vitro and in vivo studies summarized below.

Cell culture experiments revealed that proliferation of osteoblastic MC3T3-E1 cells was suppressed on Ap-CS compared to that on CS, although cyto-compatibilities of CS and Ap-CS were comparable in the initial stage of culture (on Day 1) (Figure 5A and 5B). These results are consistent with the results of the previous report[35]. We hypothesize that the apatite coating on Ap-CS suppresses cell proliferation owing to this matrix's osteogenic properties and Ca-releasing ability, as indicated by the experimental evidence in the present and previous reports, as detailed below. Some osteoconductive materials, including sintered HA, are known to stimulate the osteogenic differentiation of cells rather than to support cellular proliferation, which leads to bone formation[43, 44]. The Ca-release test in the present work showed that Ap-CS releases Ca, in contrast to CS (for

which no Ca release was seen) (Figure 4B). Maeno et al. reported that high concentrations of Ca suppress cell proliferation in a dose-dependent manner[45]. Previous reports have revealed that relatively high concentrations of Ca enhance the expression of genes regulated by osteogenic promoters, enhancing subsequent osteogenic differentiation of mesenchymal stem cells[46, 47]. The enhancement of osseous differentiation by the apatite coating was evident in the present work from the significantly higher expression levels of osteogenic markers *Ibsp* and *Bglap1* in MC3T3-E1 cells cultured on Ap-CS (compared to those in cells cultured on CS) (Figure 5C). Bone sialoprotein and OCN (which are related to Ibsp and Bglap1, respectively) are non-collagenous proteins that are expressed by cells undergoing osteogenic differentiation[48, 49].

We confirmed that Ap-CS augmented new bone formation in the rat skull compared to CS (Figures 6 and 7). It is likely that the apatite coating on Ap-CS enhances penetration of cells into the scaffold and encourages the osteogenic differentiation of these cells, consequently promoting new bone formation in vivo. The enhanced cell-ingrowth into Ap-CS was confirmed in the rat skull as well as in the rat subcutaneous tissue (as previously reported)[35]. Immunohistochemical staining at 10 days after implantation revealed the presence of a larger number of CD163-positive macrophages (M2 macrophages) in the residue of Ap-CS than in the CS residue (Figure 6). M2 macrophages are associated with immunosuppression and are known to enhance tissue repair, remodeling, and wound healing[50]. In addition, M2 macrophages secrete an osteoinductive factor; bone morphogenetic protein-2, along with vascular endothelial growth factor and transforming growth factor-β[51]. Indeed, more RUNX-2- and OCN-positive osteoblast progenitors were observed in the Ap-CS residue than in the CS residue (Figure 6). Sugimoto et al. reported the migration of monocytes and osteoblastic MC3T3-

E1 cells toward higher Ca concentrations[52]. Release of Ca from the apatite coating of Ap-CS may play a key role in the behaviors of macrophages and osteogenesis-related cells and consequently in bone tissue formation.

An in vivo study using a dog periodontal furcation defect model demonstrated the potential of Ap-CS for promoting alveolar bone regeneration compared to CS (Figure 8). Even though this work was a pilot study with a limited number of samples, ankylosis was not observed, and a periodontal ligament space was observed consistently along the tooth root in the Ap-CS group, suggesting the formation of the periodontal attachment apparatus, including cementum, periodontal ligament, and alveolar bone proper in the tested samples. Multiple investigators have reported periodontal regeneration using sintered CaP ceramics as an osteogenic scaffold[53]. However, periodontal regeneration with sintered CaP ceramics often is insufficient in regeneration speed and/or quality of the regenerated tissue, most likely due to the slow resorption rate of these ceramics[54]. Ogawa et al. succeeded in rapid periodontal tissue reconstruction by combining fine particles of β-TCP with a collagen scaffold[55]. In the present study, we propose another approach, i.e., using low-crystalline apatite coating over a porous scaffold of collagen. Despite the higher resistance to collagenase degradation (Figure 4C), Ap-CS was degraded and resorbed more rapidly than CS, while being replaced with the regenerated bone tissue (Figure 7). The early resorption of Ap-CS likely reflects enhanced cellular responses to the scaffold owing to the relatively soluble, Ca-releasing low-crystalline apatite coating.

As described above, osteogenic properties and bioresorbability of Ap-CS are suggested in this study. However, the present in vivo study using a beagle dog has limitations of insufficient sample numbers and experimental conditions. Further studies,

such as shorter- and longer-term experiments, immunohistochemical analysis and safety assessment, are required to verify the usefulness of Ap-CS as a scaffold for periodontal regenerative therapy.

5. Conclusion

Owing to the surface apatite coating prepared by the plasma- and precursor-assisted biomimetic process, Ap-CS exhibited increased water absorption, Ca release, lysozyme adsorption, collagenase resistance, and osteogenic properties compared to CS. In rat experiments, Ap-CS provided significantly enhanced skull bone formation and faster resorption compared to CS. In addition, Ap-CS demonstrated the potential to regenerate alveolar bone in a dog premolar furcation defect. Although further studies are needed, Ap-CS is a potential candidate for an osteogenic and bioresorbable scaffold for periodontal tissue reconstruction.

6. Conflicts of interest

The authors have no conflict of interest to declare.

7. Acknowledgments

The authors acknowledge Toshihiko Iwanaga (Department of Histology and Cytology, Faculty of Medicine, Hokkaido University) and Ms. Ikuko Sakamaki (Nanomaterials Research Institute, National Institute of Advanced Industrial Science and Technology (AIST)) for their technical assistance. This work was supported by JSPS KAKENHI (Grant Numbers 16K11822 and 18F18106).

8. Author Contributions

Yukimi KANEMOTO: Data Curation; formal analysis (equal); investigation (equal); methodology (equal); validation (equal); visualization (lead); writing – original draft preparation (lead). Hirofumi MIYAJI: Conceptualization (equal); formal analysis (supporting); funding acquisition (equal); investigation (supporting); methodology (equal); project administration (equal); supervision (equal); validation (equal); visualization (supporting); writing – review & editing (equal). Erika NISHIDA: Formal analysis (supporting); investigation (equal); validation(supporting). Saori MIYATA: Formal analysis (supporting); investigation (equal); validation (supporting). Kayoko MAYUMI: investigation (supporting); validation (supporting). Yuto YOSHINO: Investigation (supporting); validation (supporting). Akihito KATO: Formal analysis (supporting); funding acquisition (supporting); investigation (supporting); writing – review & editing (supporting). Tsutomu SUGAYA: Writing – review & editing (supporting). Tsukasa AKASAKA: Funding acquisition (supporting); resources (lead); writing – review & editing (supporting). Joseph Nathanael ARPUTHARAJ: Resources (equal); writing – review & editing (supporting). Syama SANTHAKUMAR: Resources (equal); writing – review & editing (supporting). Ayako OYANE: Conceptualization (equal); funding acquisition (equal); investigation (equal); methodology (equal); project administration (equal); supervision (equal); writing – review & editing (equal).

9. References

1 Larsson L, Decker AM, Nibali L, Pilipchuk SP, Berglundh T, Giannobile WV. Regenerative medicine for periodontal and peri-implant diseases. *J Dent Res*, 2016; **95**(3): 255-266. doi:10.1177/0022034515618887

2 Fawzy El-Sayed KM, Mekhemar MK, Beck-Broichsitter BE, Bähr T, Hegab M, Receveur J, Heneweer C, Becker ST, Wiltfang J, Dörfer CE. Periodontal

regeneration employing gingival margin-derived stem/progenitor cells in conjunction with IL-1ra-hydrogel synthetic extracellular matrix. *J Clin Periodontol*, 2015; **42**(5): 448-457. doi: 10.1111/jcpe.12401.

3 Tobita M, Mizuno H. Adipose-derived stem cells and periodontal tissue engineering. *Int J Oral Maxillofac Implants*, 2013; **28**(6): e487-493. doi: 10.11607/jomi.te29.

4 Onizuka S, Iwata T. Application of periodontal ligament-derived multipotent mesenchymal stromal cell sheets for periodontal regeneration. *Int J Mol Sci*, 2019; **20**(11): 2796. doi: 10.3390/ijms20112796.

5 Giannobile WV, Lee CS, Tomala MP, Tejeda KM, Zhu Z. Platelet-derived growth factor (PDGF) gene delivery for application in periodontal tissue engineering. *J Periodontol*, 2001; **72**(6) :815-823. doi: 10.1902/jop.2001.72.6.815.

6 Hovey LR, Jones AA, McGuire M, Mellonig JT, Schoolfield J, Cochran DL. Application of periodontal tissue engineering using enamel matrix derivative and a human fibroblast-derived dermal substitute to stimulate periodontal wound healing in Class III furcation defects. *J Periodontol*, 2006; **77**(5): 790-799. doi: 10.1902/jop.2006.030264.

7 Murakami S. Periodontal tissue regeneration by signaling molecule(s): what role does basic fibroblast growth factor (FGF-2) have in periodontal therapy? *Periodontol 2000*, 2011; **56**(1): 188-208. doi: 10.1111/j.1600-0757.2010.00365.x.

8 Kang W, Liang Q, Du L, Shang L, Wang T, Ge S. Sequential application of bFGF and BMP-2 facilitates osteogenic differentiation of human periodontal ligament stem cells. *J Periodontal Res*, 2019; **54**(4): 424-434. doi: 10.1111/jre.12644.

9 Kosen Y, Miyaji H, Kato A, Sugaya T, Kawanami M. Application of collagen hydrogel/sponge scaffold facilitates periodontal wound healing in class II furcation defects in beagle dogs. *J Periodontal Res*, 2012; **47**(5): 626-634. doi: 10.1111/j.1600-0765.2012.01475.x.

10 Sheikh Z, Hamdan N, Ikeda Y, Grynpas M, Ganss B, Glogauer M. Natural graft tissues and synthetic biomaterials for periodontal and alveolar bone reconstructive applications: a review. *Biomater Res*, 2017; **21**: 9. doi: 10.1186/s40824-017-0095-5.

11 Kawamoto K, Miyaji H, Nishida E, Miyata S, Kato A, Tateyama A, Furihata T, Shitomi K, Iwanaga T, Sugaya T. Characterization and evaluation of graphene oxide scaffold for periodontal wound healing of class II furcation defects in dog. *Int J Nanomedicine*, 2018; **13**: 2365-2376. doi: 10.2147/IJN.S163206.

12 Min Z, Shichang Z, Chen X, Yufang Z, Changqing Z. 3D-printed dimethyloxallyl glycine delivery scaffolds to improve angiogenesis and osteogenesis. *Biomater Sci*, 2015; **3**(8): 1236-1244. doi: 10.1039/c5bm00132c.

13 Kakar A, Rao BHS, Hegde S, Deshpande N, Lindner A, Nagursky H, Patney A, Mahajan H. Ridge preservation using an in situ hardening biphasic calcium phosphate (β-TCP/HA) bone graft substitute-a clinical, radiological, and histological study. *Int J Implant Dent*, 2017; **3**(1): 25. doi: 10.1186/s40729-017-0086-2.

14 Dewi AH, Ana ID. The use of hydroxyapatite bone substitute grafting for alveolar ridge preservation, sinus augmentation, and periodontal bone defect: A systematic review. *Heliyon*, 2018; **4**(10): e00884. doi: 10.1016/j.heliyon.2018.e00884.

15 Shu R, McMullen R, Baumann MJ, McCabe LR. Hydroxyapatite accelerates differentiation and suppresses growth of MC3T3-E1 osteoblasts. *J Biomed Mater Res A*, 2003; **67**(4): 1196-1204. doi: 10.1002/jbm.a.20021.

16 Murakami S, Miyaji H, Nishida E, Kawamoto K, Miyata S, Takita H, Akasaka T, Fugetsu B, Iwanaga T, Hongo H, Amizuka N, Sugaya T, Kawanami M. Dose effects of beta-tricalcium phosphate nanoparticles on biocompatibility and bone conductive ability of three-dimensional collagen scaffolds. *Dent Mater J*, 2017; **36**(5): 573-583. doi: 10.4012/dmj.2016-295.

17 Hoogendoorn HA, Renooij W, Akkermans LM, Visser W, Wittebol P. Long-term study of large ceramic implants (porous hydroxyapatite) in dog femora. *Clin Orthop Relat Res*, 1984; **(187)**: 281-288.

18 Kurashina K, Kurita H, Wu Q, Ohtsuka A, Kobayashi H. Ectopic osteogenesis with biphasic ceramics of hydroxyapatite and tricalcium phosphate in rabbits. *Biomaterials,* 2002; **23**(2): 407-412. doi: 10.1016/s0142-9612(01)00119-3.

19 Chang HY, Tuan WH, Lai PL. Biphasic ceramic bone graft with biphasic degradation rates. *Mater Sci Eng C Mater Biol Appl*, 2021; **118**: 111421. doi: 10.1016/j.msec.2020.111421.

20 Kamakura S, Sasano Y, Shimizu T, Hatori K, Suzuki O, Kagayama M, Motegi K. Implanted octacalcium phosphate is more resorbable than beta-tricalcium phosphate and hydroxyapatite. *J Biomed Mater Res*, 2002; **59**(1): 29-34. doi: 10.1002/jbm.1213.

21 Sawada K, Nakahara K, Haga-Tsujimura M, Iizuka T, Fujioka-Kobayashi M, Igarashi K, Saulacic N. Comparison of three block bone substitutes for bone regeneration: long-term observation in the beagle dog. *Odontology*, 2018; **106**(4): 398-407. doi: 10.1007/s10266-018-0352-7.

22 Liu Y, Luo D, Wang T. Hierarchical structures of bone and bioinspired bone tissue engineering. *Small*, 2016; **12**(34): 4611-4632. doi: 10.1002/smll.201600626.

23 Zhou C, Ye X, Fan Y, Ma L, Tan Y, Qing F, Zhang X. Biomimetic fabrication of a three-level hierarchical calcium phosphate/collagen/hydroxyapatite scaffold for bone tissue engineering. *Biofabrication*, 2014; **6**(3): 035013. doi: 10.1088/1758-

5082/6/3/035013.

24 Sadowska JM, Guillem-Marti J, Montufar EB, Espanol M, Ginebra MP. Biomimetic versus sintered calcium phosphates: The in vitro behavior of osteoblasts and mesenchymal stem cells. *Tissue Eng Part A*, 2017; **23**(23-24): 1297-1309. doi: 10.1089/ten.TEA.2016.0406.

25 Loszach M, Gitzhofer F. Induction suspension plasma sprayed biological-like hydroxyapatite coatings. *J Biomater Appl*, 2015; **29**(9): 1256-1271. doi: 10.1177/0885328214562435.

26 Levingstone TJ, Ardhaoui M, Benyounis K, Looney L, Stokes JT. Plasma sprayed hydroxyapatite coatings: Understanding process relationships using design of experiment analysis. *Surf Coat Technol*, 2015; **283**: 29-36. doi: 10.1016/j.surfcoat.2015.10.044

27 Nishikawa H, Hasegawa T, Miyake A, Tashiro Y, Hashimoto Y, Blank DH, Rijnders G. Relationship between the Ca/P ratio of hydroxyapatite thin films and the spatial energy distribution of the ablation laser in pulsed laser deposition. *Mater Lett*, 2016; **165**: 95-98. doi: 10.1016/j.matlet.2015.11.115

28 Rau JV, Cacciotti I, Laureti S, Fosca M, Varvaro G, Latini A. Bioactive, nanostructured Si-substituted hydroxyapatite coatings on titanium prepared by pulsed laser deposition. *J Biomed Mater Res B Appl Biomater*, 2015; **103**(8): 1621-31. doi: 10.1002/jbm.b.33344.

29 Ivanova AA, Surmeneva MA, Surmenev RA, Depla D. Influence of deposition conditions on the composition, texture and microstructure of RF-magnetron sputter-deposited hydroxyapatite thin films. *Thin Sol Fl*, 2015; 591 part B: 368-374. doi:10.1016/j.tsf.2015.03.058

30 Nathanael AJ, Yuvakkumar R, Hong SI, Oh TH. Novel zirconium nitride and hydroxyapatite nanocomposite coating: detailed analysis and functional properties. *ACS Appl Mater Interf*, 2014; **6**(12): 9850-9857. doi: 10.1021/am5023557.

31 Oyane A, Wang X, Sogo Y, Ito A, Tsurushima H. Calcium phosphate composite layers for surface-mediated gene transfer. *Acta Biomater*, 2012; **8**(6): 2034-2046. doi: 10.1016/j.actbio.2012.02.003.

32 Oyane A, Uchida M, Yokoyama Y, Choong C, Triffitt J, Ito A. Simple surface modification of poly(ε-caprolactone) to induce its apatite-forming ability. *J Biomed Mater Res A*, 2005; **75**(1): 138-145. doi: 10.1002/jbm.a.30397.

33 Yokoyama Y, Oyane A, Ito A. Preparation of a bonelike apatite-polymer fiber composite using a simple biomimetic process. *J Biomed Mater Res B Appl Biomater*, 2008; **86**(2): 341-352. doi: 10.1002/jbm.b.31025.

34 Suzuki Y, Oyane A, Ikeno F, Lyons JK, Yeung AC. Development of animal model for calcified chronic total occlusion. *Catheter Cardiovasc Interv*, 2009; **74**(3): 468-475. doi: 10.1002/ccd.22024.

35 Nathanael AJ, Oyane A, Nakamura M, Sakamaki I, Nishida E, Kanemoto Y, Miyaji H. In vitro and in vivo analysis of mineralized collagen-based sponges prepared by a plasma- and precursor-assisted biomimetic process. *ACS Appl Mater Interfaces*, 2017; **9**(27): 22185-22194. doi: 10.1021/acsami.7b04776.

36 Gu Y, Bai Y, Zhang D. Osteogenic stimulation of human dental pulp stem cells with a novel gelatin-hydroxyapatite-tricalcium phosphate scaffold. *J Biomed Mater Res A*, 2018; **106**(7):1851-1861. doi: 10.1002/jbm.a.36388.

37 Pfaffl MW. A new mathematical model for relative quantification in real-time RT-PCR. *Nucleic Acids Res*, 2001; **29**(9): e45. doi: 10.1093/nar/29.9.e45.

38 Schmittgen TD, Zakrajsek BA. Effect of experimental treatment on housekeeping gene expression: validation by real-time, quantitative RT-PCR. *J Biochem Biophys Methods*, 2000; **46**(1-2): 69-81. doi: 10.1016/s0165-022x(00)00129-9.

39 Feller L, Jadwat Y, Khammissa RA, Meyerov R, Schechter I, Lemmer J. Cellular responses evoked by different surface characteristics of intraosseous titanium implants. *Biomed Res Int*, 2015; **2015**: 171945. doi: 10.1155/2015/171945.

40 Galli C, Parisi L, Piergianni M, Smerieri A, Passeri G, Guizzardi S, Costa F, Lumetti S, Manfredi E, Macaluso GM. Improved scaffold biocompatibility through anti-Fibronectin aptamer functionalization. *Acta Biomater*, 2016; **42**: 147-156. doi: 10.1016/j.actbio.2016.07.035.

41 Wang S, Li R, Xu Y, Xia D, Zhu Y, Yoon J, Gu R, Liu X, Zhao W, Zhao X, Liu Y, Sun Y, Zhou Y. Fabrication and Application of a 3D-Printed Poly-ε-Caprolactone Cage Scaffold for Bone Tissue Engineering. *Biomed Res Int*, 2020; **2020**: 2087475. doi: 10.1155/2020/2087475.

42 Espanol M, Casals I, Lamtahri S, Valderas MT, Ginebra MP. Assessment of protein entrapment in hydroxyapatite scaffolds by size exclusion chromatography. *Biointerphases*, 2012; **7**(1-4): 37. doi: 10.1007/s13758-012-0037-7.

43 Kim SH, Oh SA, Lee WK, Shin US, Kim HW. Poly(lactic acid) porous scaffold with calcium phosphate mineralized surface and bone marrow mesenchymal stem cell. *Mater Sci Eng C*, 2011; **31**(3): 612-619. doi:10.1016/j.msec.2010.11.028.

44 Raucci MG, Giugliano D, Alvarez-Perez MA, Ambrosio L. Effects on growth and osteogenic differentiation of mesenchymal stem cells by the strontium-added sol-gel hydroxyapatite gel materials. *J Mater Sci Mater Med*, 2015; **26**(2): 90. doi: 10.1007/s10856-015-5436-0.

45 Maeno S, Niki Y, Matsumoto H, Morioka H, Yatabe T, Funayama A, Toyama Y, Taguchi T, Tanaka J. The effect of calcium ion concentration on osteoblast viability, proliferation and differentiation in monolayer and 3D culture. *Biomaterials*, 2005; **26**(23): 4847-4855. doi: 10.1016/j.biomaterials.2005.01.006.

46 Lee MN, Hwang HS, Oh SH, Roshanzadeh A, Kim JW, Song JH, Kim ES, Koh JT. Elevated extracellular calcium ions promote proliferation and migration of mesenchymal stem cells via increasing osteopontin expression. *Exp Mol Med*, 2018; **50**(11): 1-16. doi: 10.1038/s12276-018-0170-6.

47 Yanai R, Tetsuo F, Ito S, Itsumi M, Yoshizumi J, Maki T, Mori Y, Kubota Y, Kajioka S. Extracellular calcium stimulates osteogenic differentiation of human adipose-derived stem cells by enhancing bone morphogenetic protein-2 expression. *Cell Calcium*, 2019; **83**: 102058. doi: 10.1016/j.ceca.2019.102058.

48 Vincent K, Durrant MC. A structural and functional model for human bone sialoprotein. *J Mol Graph Model*, 2013; **39**: 108-117. doi: 10.1016/j.jmgm.2012.10.007.

49 Weinreb M, Shinar D, Rodan GA. Different pattern of alkaline phosphatase, osteopontin, and osteocalcin expression in developing rat bone visualized by in situ hybridization. *J Bone Miner Res*, 1990; **5**(8): 831-842. doi: 10.1002/jbmr.5650050806.

50 Mantovani A, Biswas SK, Galdiero MR, Sica A, Locati M. Macrophage plasticity and polarization in tissue repair and remodelling. *J Pathol*, 2013; **229**(2): 176-185. doi: 10.1002/path.4133.

51 Chen Z, Mao X, Tan L, Friis T, Wu C, Crawford R, Xiao Y. Osteoimmunomodulatory properties of magnesium scaffolds coated with β-tricalcium phosphate. *Biomaterials*, 2014; **35**(30): 8553-8565. doi: 10.1016/j.biomaterials.2014.06.038.

52 Sugimoto T, Kanatani M, Kano J, Kaji H, Tsukamoto T, Yamaguchi T, Fukase M, Chihara K. Effects of high calcium concentration on the functions and interactions of osteoblastic cells and monocytes and on the formation of osteoclast-like cells. *J Bone Miner Res*, 1993; **8**(12): 1445-1452. doi: 10.1002/jbmr.5650081206.

53 Shue L, Yufeng Z, Mony U. Biomaterials for periodontal regeneration: a review of ceramics and polymers. *Biomatter*, 2012; **2**(4): 271-277. doi: 10.4161/biom.22948.

54 Yoshinuma N, Sato S, Fukuyama T, Murai M, Ito K. Ankylosis of nonresorbable hydroxyapatite graft material as a contributing factor in recurrent periodontitis. *Int J Periodontics Restorative Dent*, 2012; **32**(3): 331-336.

55 Ogawa K, Miyaji H, Kato A, Kosen Y, Momose T, Yoshida T, Nishida E, Miyata S,

Murakami S, Takita H, Fugetsu B, Sugaya T, Kawanami M. Periodontal tissue engineering by nano beta-tricalcium phosphate scaffold and fibroblast growth factor-2 in one-wall infrabony defects of dogs. *J Periodontal Res*, 2016; **51**(6): 758-767. doi: 10.1111/jre.12352.

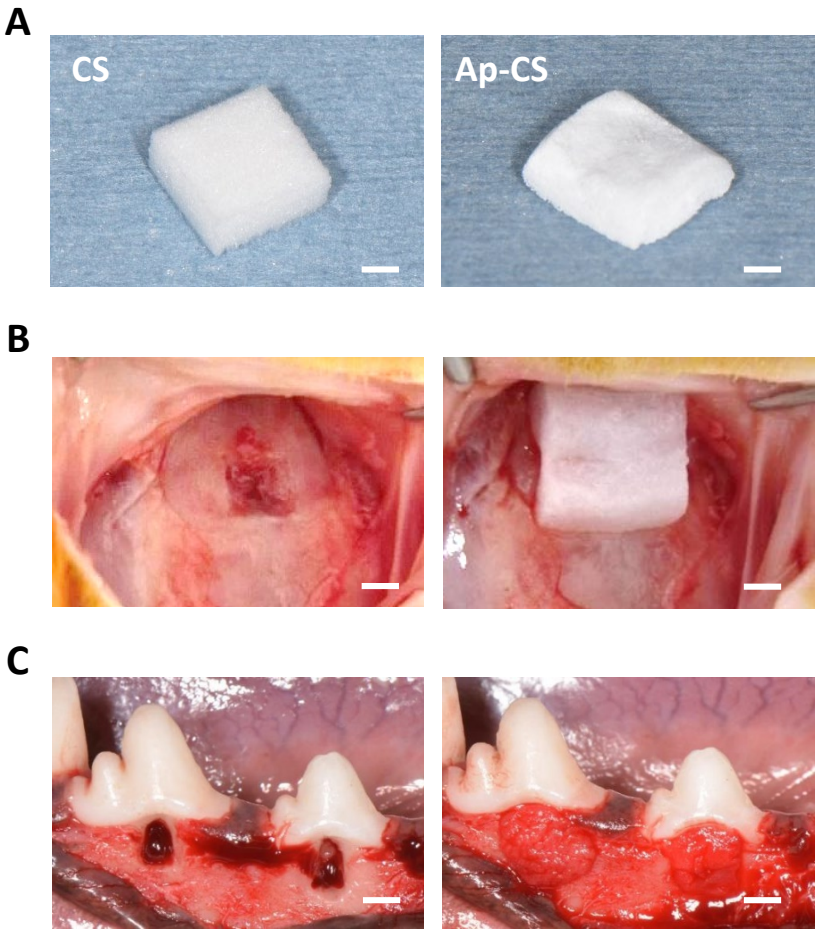

Figure 1 Scaffolds and implantation procedures in dog

(A) Digital images of the scaffolds: CS (left) and Ap-CS (right). Scale bar represents 2 mm. (B) Digital images of decorticated region before (left) and after (right) being covered with the scaffold. Scale bar represents 2 mm. (C) Digital images of surgically created premolar furcation lesions before (left) and after (right) implantation of the scaffolds. Scale bar represents 3 mm.

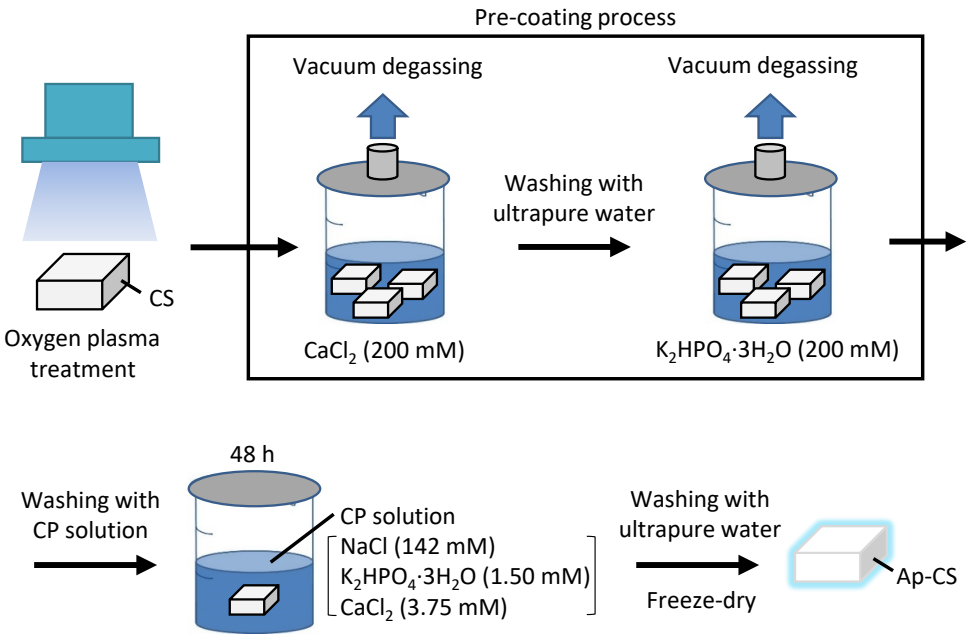

Figure 2 Procedures for preparation of Ap-CS

Plasma- and precursor-assisted biomimetic process for low-crystalline apatite coating of CS.

Abbreviations: Ap-CS, apatite-coated collagen scaffold; CP, supersaturated calcium phosphate; CS, collagen scaffold.

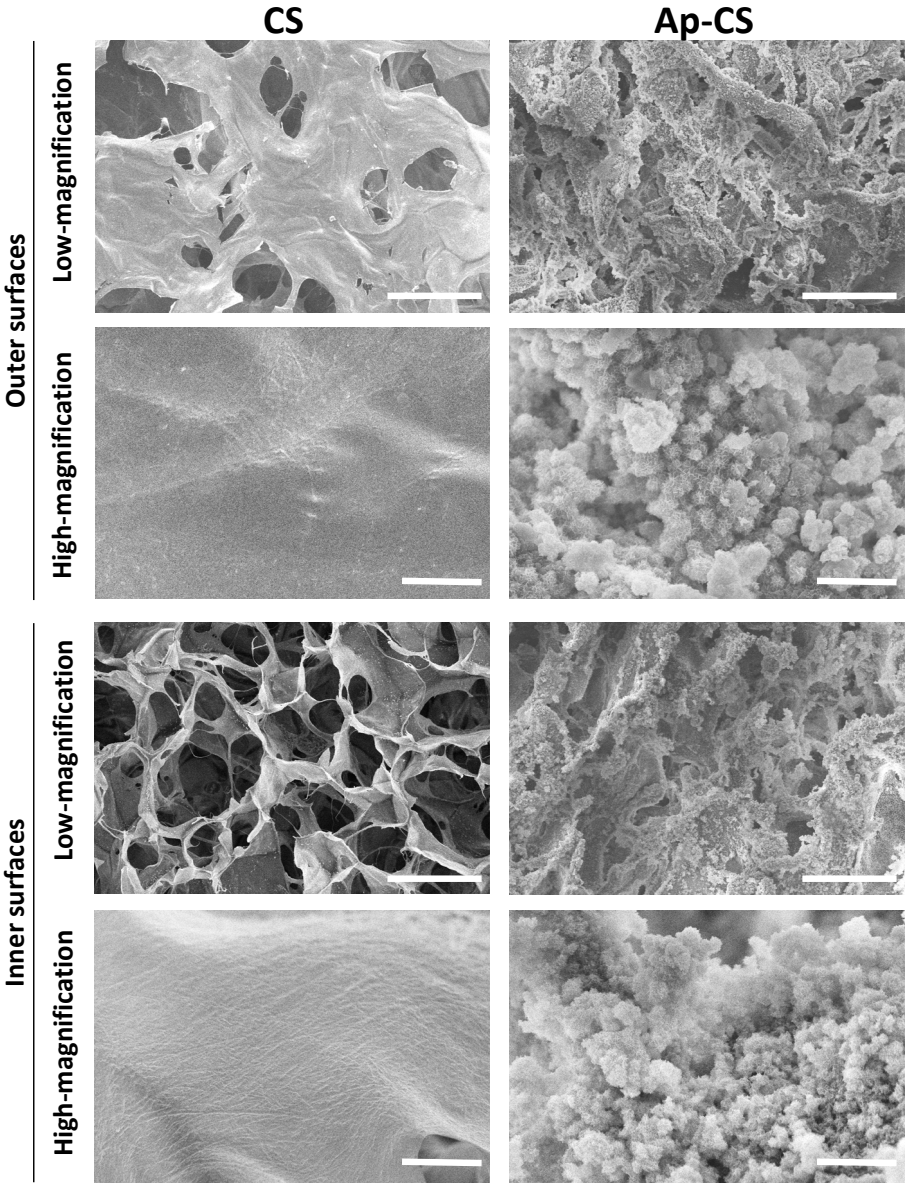

Figure 3 SEM observation of the scaffolds

SEM images of outer (upper two rows) and inner (lower two rows) surfaces of CS (left) and Ap-CS (right). Scale bars represent 100 μm in lower magnification images and 5 μm in higher magnification images.

Abbreviations: Ap-CS, apatite-coated collagen scaffold; CS, collagen scaffold; SEM, scanning electron microscope.

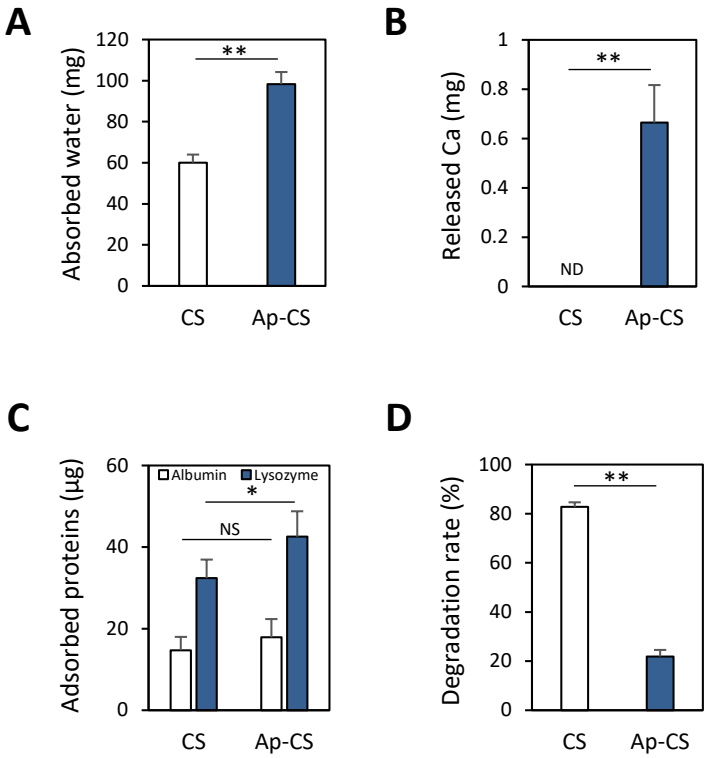

Figure 4 Physicochemical characterization of the scaffolds

In vitro characteristics of CS and Ap-CS: (A) amount of absorbed water, (B) amount of released Ca, (C) amounts of adsorbed proteins (albumin and lysozyme), and (D) enzymatic degradation rate (n=6, mean + standard deviation). *: $P<0.05$, **: $P<0.01$. Statistical analysis: two-tailed non-paired Student's t-test.

Abbreviations: Ap-CS, apatite-coated collagen scaffold; CS, collagen scaffold; ND, not detected, NS; Not significant.

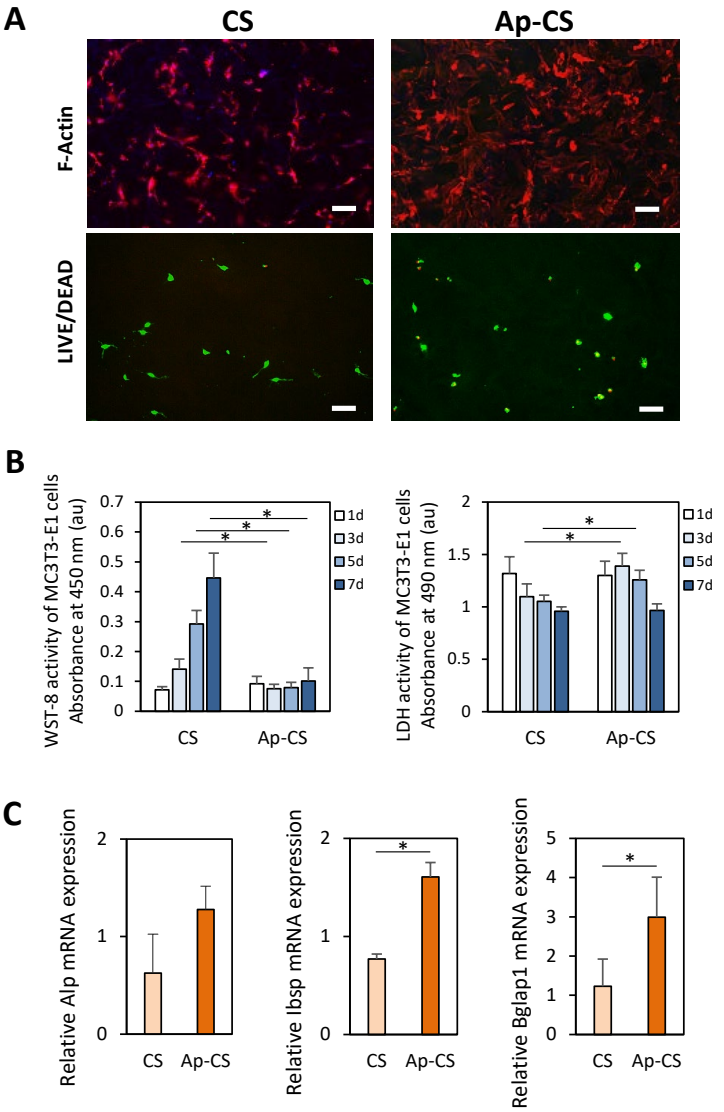

Figure 5 Cell culture experiments

(A) Fluorescence microscopic images of MC3T3-E1 cells cultured on CS (left) and Ap-CS (right) for 24 hours. Scale bar represents 100 μm. F-actin staining (stained red). LIVE/DEAD BacLight staining (live and dead cells were stained green and red, respectively). (B) WST-8 (left) and LDH (right) activity of MC3T3-E1 cells cultured on CS and Ap-CS for 1, 3, 5, and 7 days (n=5, mean + standard deviation). *: $P<0.05$. Statistical analysis: two-tailed one-way ANOVA with post hoc Tukey HSD test. (C) RT-PCR results; relative (to *Gapdh*) expression levels of *Alp* (left), *Ibsp* (center), and *Bglap1* (right) in MC3T3-E1 cells cultured on CS and Ap-CS for 14 days (n=3, mean + standard deviation). *: $P<0.05$. Statistical analysis: two-tailed non-paired Student's t-test.

Abbreviations: Ap-CS, apatite-coated collagen scaffold; CS, collagen scaffold; LDH, lactate dehydrogenase; RT-PCR, reverse transcription polymerase chain reaction; WST-8, water-soluble tetrazolium salts-8.

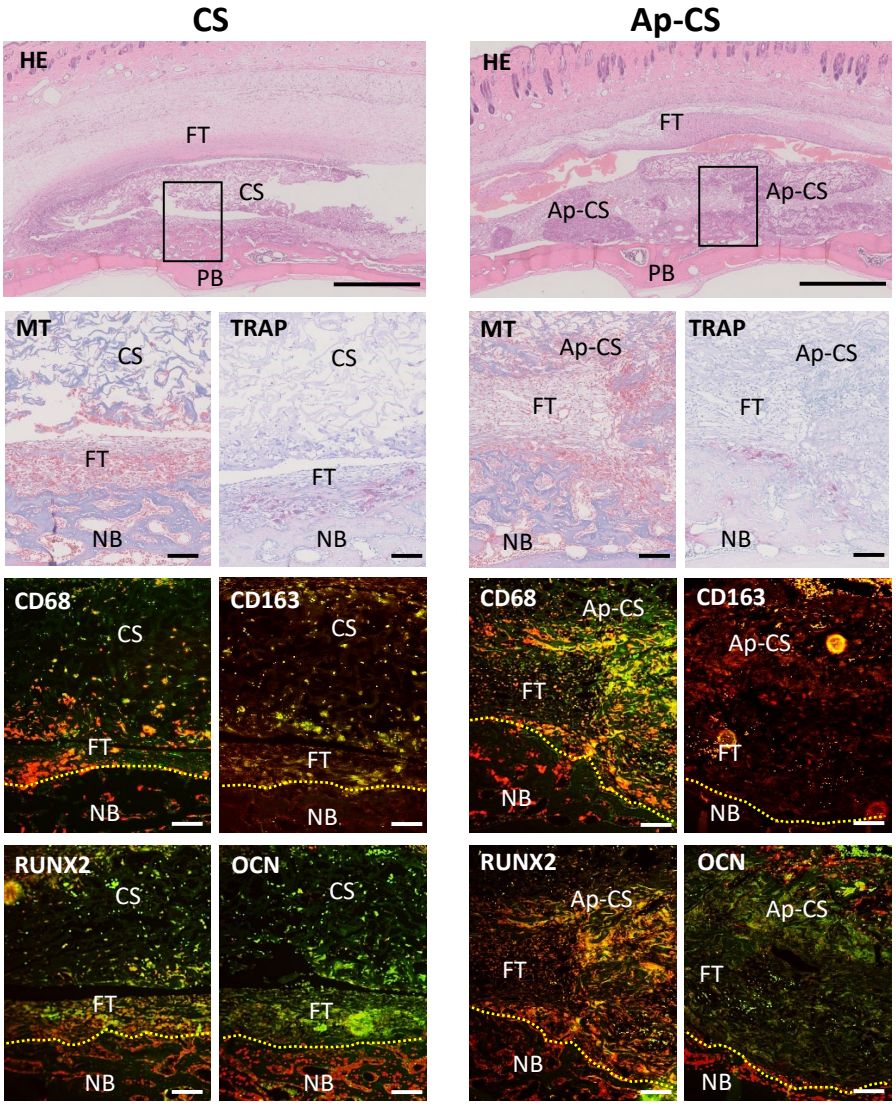

Figure 6 Immunohistochemical observation of a rat skull 10 days after implantation of the scaffolds

Optical (upper two rows) and fluorescence (lower two rows) microscopic images of the CS (left) and Ap-CS (right) groups. Staining was performed using HE, MT, and TRAP; immunostaining in red was performed with antibodies against CD68, CD163, RUNX2, and OCN, and that in green was performed against nuclei. The framed area of the HE-stained tissue image was about the same region of other images. Scale bar represents 1 mm in HE images and 100 μm in others.

Abbreviations: Ap-CS, apatite-coated collagen scaffold; CS, collagen scaffold; FT, fibrous connective tissue; HE, hematoxylin–eosin; MT, Masson's trichrome; NB, newly formed bone; OCN, osteocalcin; PB, pre-existing bone; RUNX2, runt-related transcription factor 2; TRAP, tartrate-resistant acid phosphatase.

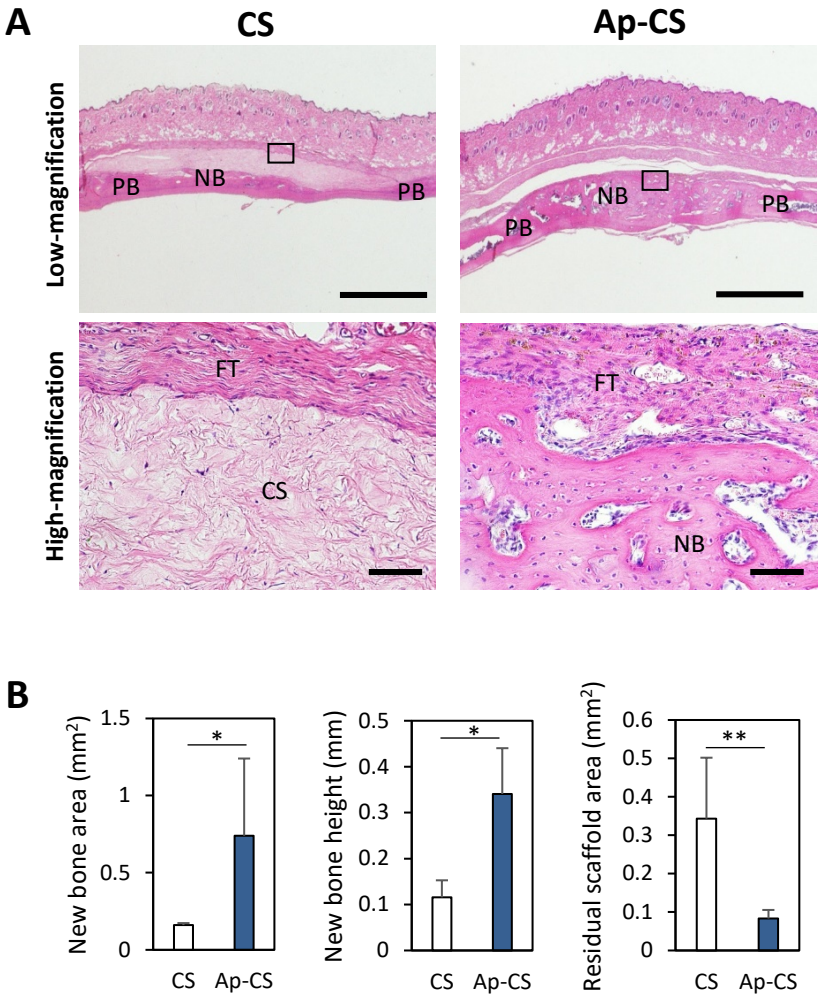

Figure 7 Histological observation of a rat skull 35 days after implantation of the scaffolds

(A) Histological images of the CS (left) and Ap-CS (right) groups. High-magnification images are magnified images of the framed areas in low-magnification images. Scale bars represent 2 mm in low-magnification images and 100 μm in high-magnification images. Hematoxylin-eosin staining. (B) Histometric results: area (left) and height (center) of the newly formed bone, and area of the residual scaffold (right) (n=5, mean + standard deviation). *: $P<0.05$, **: $P<0.01$. Statistical analysis: two-tailed non-paired Student's t-test.

Abbreviations: Ap-CS, apatite-coated collagen scaffold; CS, collagen scaffold; FT, fibrous connective tissue; NB, newly formed bone; PB, pre-existing bone.

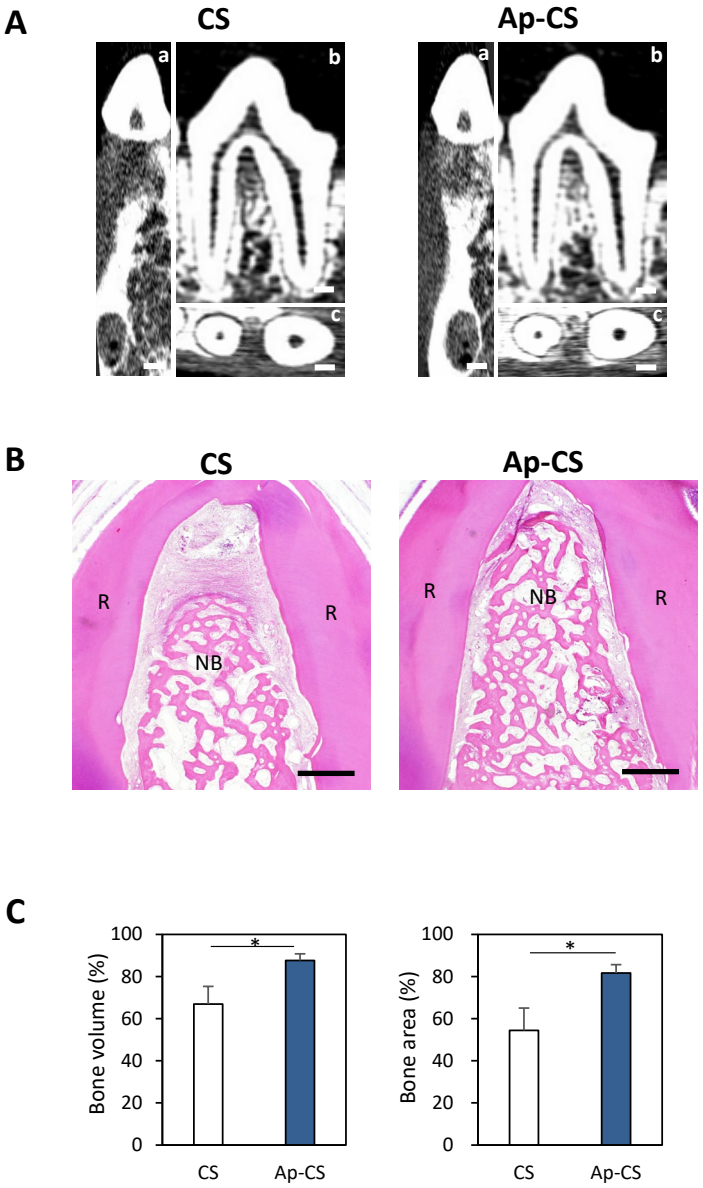

Figure 8 Micro-CT and histological observation of dog premolar furcation 35 days after implantation of the scaffolds

(A) Sagittal (a), transverse (b) and horizontal (c) planes of micro-CT images of the CS (left) and Ap-CS (right) groups. Scale bar represents 2 mm. (B) Histological images of the CS (left) and Ap-CS (right) groups. Scale bar represents 1 mm. Hematoxylin-eosin staining. (C) The percentages of bone volume (left) and the percentages of bone area (right) of the CS and Ap-CS groups (n=3, mean + standard deviation). *: $P<0.05$. Statistical analysis: two-tailed non-paired Student's t-test.

Abbreviations: Ap-CS, apatite-coated collagen scaffold; CS, collagen scaffold; CT, computed tomography; NB, newly formed bone; R, tooth root.